Astron. Astrophys. 338, 301–310 (1998)

ASTRONOMY
AND
ASTROPHYSICS

Hanle-Zeeman scattering matrix

J.O. Stenflo

Institute of Astronomy, ETH Zentrum, CH-8092 Zũrich, Switzerland

Received 15 June 1998 / Accepted 2 July 1998

Abstract. A theory is presented that allows the Mueller matrix for coherent scattering to be calculated for arbitrary magnetic fields, atomic multiplets, and scattering transitions (Rayleigh or Raman scattering). For the special case of a normal Zeeman triplet (a $J = 0 \rightarrow 1 \rightarrow 0$ scattering transition) a compact analytical form for the scattering matrix is given, which allows us to better see how the various field-strength regimes are connected. A number of limiting cases are retrieved from the general theory, including the weak-field Hanle phase matrix, the polarization of forbidden coronal lines (strong-field limit), "thermal" radiation (emission vector in LTE) and incoherent scattering. The analytical form for the transition of the Hanle effect from the line core (where it is present) to the line wings (where it is absent) is given.

Key words: atomic processes – polarization – scattering – Sun: magnetic fields – Sun: atmosphere – radiative transfer

1. Introduction

The scattering polarization in the solar spectrum that has recently become accessible to systematic exploration (Stenflo & Keller 1996, 1997) has opened a new window with rich possibilities for spectroscopy and diagnostics of the Sun. It provides us with a second solar spectrum that is a sensitive function of the strength and geometry of the magnetic fields in a parameter domain that is inaccessible to ordinary Zeeman-effect observations (Stenflo et al. 1998; Bianda et al. 1998), and therefore has potential to significantly advance our understanding of solar magnetism. However, the theory needed to interpret the wealth of new observed phenomena in scattering physics on the Sun is not yet fully developed or understood, although much progress has been made in recent years (cf. Stenflo 1994). It is now a challenge to establish a good theoretical foundation and to develop the adequate theoretical tools that can be used in a polarized radiative transfer formalism.

Recently the scattering matrix that describes the relation between the incident and scattered Stokes vectors has been derived for the general multi-level case of Raman scattering for entire atomic multiplets and applied to interpret observed features in the second solar spectrum (Stenflo 1997). This theory however did not deal with the problem of partial frequency redistribution (PRD), and it was given in explicit form only for the case of zero magnetic fields. Bommier (1997) has subsequently developed a PRD theory for the general case of arbitrary magnetic fields, for a two-level atom. Both these theories assume that the initial atomic state is unpolarized, while Trujillo-Bueno & Landi Degl'Innocenti (1997) and Landi Degl'Innocenti (1998) have shown how atomic polarization of the ground state through optical depopulation pumping can be significant for the interpretation of the observational data.

In the present paper we generalize the theory of Stenflo (1997) to derive the general Raman scattering matrix explicitly, not only for arbitrary atomic multiplets but also for arbitrary magnetic fields. This matrix simultaneously contains the Hanle and Zeeman effects and the intermediate field-strength regime that describes the transition between the Hanle and Zeeman effects. It also contains the detailed frequency dependence of these effects, including the transition of the Hanle effect from being present in the Doppler core to being absent in the wings. The analytical form for this frequency dependence of the Hanle effect is given explicitly.

For the case of a normal Zeeman triplet (a $J = 0 \rightarrow 1 \rightarrow 0$ scattering transition) the full and general Hanle-Zeeman scattering matrix is given in a compact analytical form that brings out both the dependence on frequency and on geometry of the various matrix elements in a simple and transparent form. This analytical version allows us to more directly see how various limiting cases can be retrieved from the general case, including the Hanle weak-field phase matrix, the scattering matrix for coronal forbidden lines (strong-field regime), and the "thermal" emission vector in the Unno (1956) theory. We also illustrate how the Stokes line profiles behave in the transition region between the Hanle and Zeeman effects for intermediately strong fields.

2. Derivation of the Mueller matrix for Raman scattering and arbitrary magnetic fields

2.1. Scattering amplitudes

The complex probability amplitude for scattering from initial magnetic substate a to final substate f via all possible intermediate substates b is given by the Kramers-Heisenberg formula

$$w_{\alpha\beta} \sim \sum_b \frac{\langle f \,|\, \hat{\boldsymbol{r}} \cdot \boldsymbol{e}_\alpha \,|\, b \rangle \langle b \,|\, \hat{\boldsymbol{r}} \cdot \boldsymbol{e}_\beta \,|\, a \rangle}{\omega_{bf} - \omega - i\gamma/2} \,. \tag{1}$$

ω is the frequency of the scattered radiation, $\hbar\omega_{bf}$ the energy difference between the excited and final states, and γ the damping constant that accounts for the broadening of the excited state (while the initial state in this formulation is assumed to be infinitely sharp). Because of energy conservation $\omega_{bf} - \omega$ could also be replaced by $\omega_{ba} - \omega'$, where ω' is the frequency of the incident radiation. The scalar products between the position operator $\hat{\boldsymbol{r}}$ (which is proportional to the dipole moment operator) and the linear unit polarization vectors $\boldsymbol{e}_{\alpha,\beta}$ for the radiation give rise to the geometrical factors $\varepsilon_q^{\alpha *}$ and ε_q^{β}, defined by

$$\varepsilon_q^\alpha = \boldsymbol{e}_q \cdot \boldsymbol{e}_\alpha \,, \tag{2}$$

where $\boldsymbol{e}_q$, $q = 0, \pm 1$, are the complex spherical unit vectors (cf. Stenflo 1994, pp. 48 and 183).

The matrix elements can be expanded via the Wigner-Eckardt theorem, which gives us (cf. Stenflo 1994, pp. 174 and 192)

$$\begin{aligned} w_{\alpha\beta} \;\sim\; & \sum_{J_b,m} (-1)^{r_{ab}+r_{fb}} \sqrt{f_{ab} f_{fb}} \, \sqrt{(2J_a+1)(2J_f+1)} \\ & \begin{pmatrix} J_b & J_f & 1 \\ -m & \mu_f & -q \end{pmatrix} \begin{pmatrix} J_b & J_a & 1 \\ -m & \mu_a & -q' \end{pmatrix} \\ & (-1)^{q-q'} \, \Phi_{m\mu_f}(\nu) \, \varepsilon_q^{\alpha *} \, \varepsilon_{q'}^{\beta} \,, \end{aligned} \tag{3}$$

where m represents the magnetic quantum number of the intermediate substate b that has total angular momentum quantum number J_b, while the initial and final levels a and f have the corresponding magnetic and J quantum numbers $\mu_{a,f}$ and $J_{a,f}$. Note that we also sum over J_b to allow for coherent superposition of substates belonging to different fine-structure components (different J, or, in the case of hyperfine structure, F values). The absorption oscillator strengths between the lower $J_{a,f}$ states and the intermediate J_b states are f_{ab} and f_{fb}, while the corresponding exponents r_{ab} and r_{fb} that determine the sign of the expression have been derived and given in Stenflo (1994, p. 199; 1997).

The area-normalized profile function

$$\Phi_{m\mu_f} = \frac{2/i}{\omega_{m\mu_f} - \omega - i\gamma/2} \,, \tag{4}$$

where

$$\begin{aligned} \omega_{m\mu_f} \;&=\; (E_m - E_{\mu_f})/\hbar \\ &=\; \omega_{bf} + (g_b m - g_f \mu_f) \, \omega_L \,, \end{aligned} \tag{5}$$

$\hbar\omega_{bf}$ is the energy difference between the upper and lower states in the absence of magnetic fields, $g_{b,f}$ the Landé factors of the intermediate and final states, ω_L the Larmor frequency, and

$$\begin{aligned} q \;&=\; \mu_f - m \,, \\ q' \;&=\; \mu_a - m \,. \end{aligned} \tag{6}$$

According to the selection rules that follow from the properties of the 3-j symbols, q and q' may be zero (for the π components) or ± 1 (for the σ components).

2.2. Scattering of the Stokes vector

Ignoring an unimportant proportionality factor, we obtain the Mueller scattering matrix $\boldsymbol{M}$ that describes the transformation of the incident to the scattered Stokes vector from

$$\boldsymbol{M} = \boldsymbol{T} \, \boldsymbol{W} \, \boldsymbol{T}^{-1} \,, \tag{7}$$

where

$$\boldsymbol{W} = \sum_{\mu_a} \rho_{\mu_a \mu_a} \sum_{\mu_f} \boldsymbol{w} \otimes \boldsymbol{w}^* \tag{8}$$

(Stenflo 1994, pp. 41, 122, and 174). The symbols $\otimes$ and $*$ stand for tensor product and complex conjugation, respectively. $\rho_{\mu_a \mu_a}$ represents the relative populations of the initial magnetic substates μ_a (diagonal density matrix elements for the initial state, normalized such that the sum over $\rho_{\mu_a \mu_a}$ is unity). It is included here to account for the possibility that the initial state may have atomic polarization (which implies a non-LTE population of the magnetic substates). To find this atomic polarization one would have to solve the statistical equilibrium equations with coherences, a problem outside the scope of the present paper. Note that the summation over μ_a and μ_f can run over magnetic substates that belong to more than one J state, to include all scattering contributions within a whole multiplet. Without initial-state polarization all $\rho_{\mu_a \mu_a}$ are equal and can therefore be omitted (since a constant of proportionality or scale factor in $\boldsymbol{W}$ is unimportant here as it disappears when the matrix $\boldsymbol{M}$ is normalized).

The matrices $\boldsymbol{T}$, $\boldsymbol{T}^{-1}$ in Eq. (7) are purely mathematical transformation matrices without physical contents:

$$\begin{aligned} \boldsymbol{T} &= \begin{pmatrix} 1 & 0 & 0 & 1 \\ 1 & 0 & 0 & -1 \\ 0 & 1 & 1 & 0 \\ 0 & -i & i & 0 \end{pmatrix} \,, \\ \boldsymbol{T}^{-1} &= \frac{1}{2} \begin{pmatrix} 1 & 1 & 0 & 0 \\ 0 & 0 & 1 & i \\ 0 & 0 & 1 & -i \\ 1 & -1 & 0 & 0 \end{pmatrix} \,. \end{aligned} \tag{9}$$

In terms of the components $w_{\alpha\beta}$ of the scattering probability in Eq. (1) the tensor product in Eq. (8) is

$$\boldsymbol{w} \otimes \boldsymbol{w}^* = \begin{pmatrix} w_{11}w_{11}^* & w_{11}w_{12}^* & w_{12}w_{11}^* & w_{12}w_{12}^* \\ w_{11}w_{21}^* & w_{11}w_{22}^* & w_{12}w_{21}^* & w_{12}w_{22}^* \\ w_{21}w_{11}^* & w_{21}w_{12}^* & w_{22}w_{11}^* & w_{22}w_{12}^* \\ w_{21}w_{21}^* & w_{21}w_{22}^* & w_{22}w_{21}^* & w_{22}w_{22}^* \end{pmatrix} . \tag{10}$$

It has the structure

$$\boldsymbol{w} \otimes \boldsymbol{w}^* = \begin{pmatrix} A & b & b^* & C \\ c & a & d & e \\ c^* & d^* & a^* & e^* \\ D & f & f^* & B \end{pmatrix} \,, \tag{11}$$

where

$$\begin{aligned} A \;&=\; |w_{11}|^2 \,, \\ B \;&=\; |w_{22}|^2 \,, \end{aligned}$$

$$
\begin{aligned}
C &= |w_{12}|^2 \,, \\
D &= |w_{21}|^2 \,, \\
a &= w_{11} w_{22}^* \,, \\
b &= w_{11} w_{12}^* \,, \\
c &= w_{11} w_{21}^* \,, \\
d &= w_{12} w_{21}^* \,, \\
e &= w_{12} w_{22}^* \,, \\
f &= w_{21} w_{22}^* \,.
\end{aligned} \tag{12}
$$

With these definitions we now transform $\boldsymbol{w} \otimes \boldsymbol{w}^*$ to the Mueller matrix $\boldsymbol{M}$, using Eq. (7). We obtain

$$
\boldsymbol{M} = \sum_{\mu_a} \rho_{\mu_a \mu_a} \sum_{\mu_f} (\, \boldsymbol{M}_Q + \mathrm{Re}\, \boldsymbol{M}_U + \mathrm{Im}\, \boldsymbol{M}_V \,) \,, \tag{13}
$$

where the matrix $\boldsymbol{M}_Q$ only describes the Stokes $I \leftrightarrow Q$ and $I \leftrightarrow I$ coupling, while $\boldsymbol{M}_U$ describes the $I \leftrightarrow U$ and $V \leftrightarrow V$ coupling, $\boldsymbol{M}_V$ the $I \leftrightarrow V$ coupling.

$$
\begin{aligned}
\boldsymbol{M}_Q &= \frac{1}{2} \begin{pmatrix} A+B+C+D & A-B-C+D & 0 & 0 \\ A-B+C-D & A+B-C-D & 0 & 0 \\ 0 & 0 & 0 & 0 \\ 0 & 0 & 0 & 0 \end{pmatrix} , \\
\boldsymbol{M}_U &= \begin{pmatrix} 0 & 0 & b+f & 0 \\ 0 & 0 & b-f & 0 \\ c+e & c-e & a+d & 0 \\ 0 & 0 & 0 & a-d \end{pmatrix} , \\
\boldsymbol{M}_V &= \begin{pmatrix} 0 & 0 & 0 & -b-f \\ 0 & 0 & 0 & -b+f \\ 0 & 0 & 0 & -a+d \\ c+e & c-e & a+d & 0 \end{pmatrix} .
\end{aligned} \tag{14}
$$

We note that this theory can deal with general Raman scattering with quantum interferences between any of the upper m, J, or F (in case of hyperfine structure) states (since the summation in Eq. (3) is done over both m and J_b), and the initial and final J states may be different. This is the general multi-level case with quantum coherences between the upper, intermediate states, but with neglect of Doppler broadening and partial redistribution, and without any explicit derivation of atomic polarization and coherences in the initial state. The initial state is also assumed to be infinitely sharp (implying an infinite life time).

2.3. Doppler broadening

Before convolving the scattering matrix $\boldsymbol{M}$ with a Gaussian it is convenient to introduce a frequency scale v in units of the Doppler width $\Delta\omega_D$:

$$
v = (\omega_0 - \omega)/\Delta\omega_D \,, \tag{15}
$$

where ω_0 is the same resonance frequency as ω_{bf} in Eq. (5). We further introduce the notation

$$
v_q = v - v_H(\mu_f, m) \,, \tag{16}
$$

where

$$
v_H(\mu_f, m) = [\, g_b \, q - (g_b - g_f) \, \mu_f \,] \, \omega_L / \Delta\omega_D \tag{17}
$$

according to Eqs. (5) and (6) and thus only dependent on q if μ_f is held fixed. Eq. (4) for $\Phi_{m\mu_f}$ can then be replaced by

$$
\Phi_q = \frac{a - i v_q}{\pi \, (\, v_q^2 + a^2)} \,, \tag{18}
$$

where the damping parameter

$$
a = \gamma / (2 \Delta\omega_D) \,. \tag{19}
$$

Φ_q is normalized such that integration over v_q gives unity.

The frequency-dependent factors in the expression for the scattering matrix $\boldsymbol{M}$ are, as seen from Eqs. (8) and (10), given by products $\Phi_q \Phi_{q'}^*$ that represent interference between different magnetic substates when $q \neq q'$. The Doppler convolution is greatly simplified if these products are first converted to sums. The conversion formula is

$$
\Phi_q \Phi_{q'}^* = \frac{1}{2\pi a} \cos\alpha_{q-q'} \; e^{i\alpha_{q-q'}} \; (\Phi_q + \Phi_{q'}^*) \,, \tag{20}
$$

where the *Hanle angle* $\alpha_{q-q'}$ is given by

$$
\tan\alpha_{q-q'} = \frac{(q - q') \, g_b \, \omega_L}{\gamma_\alpha} \,. \tag{21}
$$

We have here written γ_α instead of γ to recall that in a frequency-redistribution treatment with collisions (which we are not doing here) the γ that appears in the profile function Φ_q is not quite the same as the γ in the expression for $\tan\alpha_{q-q'}$. In Φ_q it is $\gamma = \gamma_N + \gamma_c$, while in $\tan\alpha_{q-q'}$ it is $\gamma_\alpha = \gamma_N + \gamma_c/2$ (cf. Stenflo 1994, pp. 212–213; Bommier 1997). γ_N is the natural, radiative damping constant, while γ_c is the collisional damping constant. This distinction should be remembered when computing Φ_q and $\alpha_{q-q'}$, but it does not follow from the present treatment (which does not address the frequency distribution problem when collisions are present).

Doppler broadening of Φ_q gives $\mathcal{H}(a, v_q)/\sqrt{\pi}$, where

$$
\mathcal{H}(a, v) = H(a, v) - 2iF(a, v) \,. \tag{22}
$$

$$
H(a, v) = \frac{a}{\pi} \int_{-\infty}^{+\infty} \frac{e^{-y^2} \, \mathrm{d}y}{(v - y)^2 + a^2} \tag{23}
$$

is the Voigt function, while

$$
F(a, v) = \frac{1}{2\pi} \int_{-\infty}^{+\infty} \frac{(v - y) \, e^{-y^2} \, \mathrm{d}y}{(v - y)^2 + a^2} \tag{24}
$$

is the line dispersion function.

The Doppler broadened profile product in Eq. (20) thus becomes

$$
\frac{1}{\sqrt{\pi}} \int_{-\infty}^{+\infty} \Phi_q \Phi_{q'}^* \, e^{-x^2} \, \mathrm{d}x = \frac{1}{\pi^{3/2} a} \, I_{qq'} \,, \tag{25}
$$

where

$$
I_{qq'} = \cos\alpha_{q-q'} \; e^{i\alpha_{q-q'}} \; \tfrac{1}{2} \, [\, \mathcal{H}(a, v_q) + \mathcal{H}^*(a, v_{q'}) \,] \,. \tag{26}
$$

The Hanle effect manifests itself in two main ways: depolarization and rotation of the plane of linear polarization. The

Hanle angle $\alpha_{q-q'}$ causes depolarization via the $\cos\alpha_{q-q'}$ factor, while the rotation enters through the $e^{i\alpha_{q-q'}}$ factor, since this term couples $\alpha_{q-q'}$ directly to the azimuths ϕ' and ϕ of the incident and scattered radiation. This coupling of angles can be seen directly from the expressions for the geometrical ε factors in Eq. (3), which for a spherical coordinate system with the polar axis along the magnetic field are

$$\begin{aligned}
\varepsilon_0^1 &= -\sin\theta\,,\\
\varepsilon_0^2 &= 0\,,\\
\varepsilon_\pm^1 &= \mp\mu\, e^{\pm i\phi}/\sqrt{2}\,,\\
\varepsilon_\pm^2 &= -i\, e^{\pm i\phi}/\sqrt{2}
\end{aligned} \tag{27}$$

(cf. Stenflo 1994, p. 57), if the linear polarization unit vectors $\boldsymbol{e}'_{1,2}$ and $\boldsymbol{e}_{1,2}$ are chosen to be parallel and perpendicular to the meridional planes. θ is the colatitude, $\mu = \cos\theta$, and ϕ is the azimuth angle of the radiation field. The primed angular quantities refer to the incident radiation, the unprimed to the scattered radiation. The bilinear products of the εs give rise to the factors $e^{-i(q-q')(\phi-\phi')}$, which couple to the $e^{i\alpha_{q-q'}}$ factor so that Hanle rotation is produced.

Let us for convenience introduce the notation

$$\begin{aligned}
h_{qq'} &= \tfrac{1}{2}\,[\,H(a,v_q) + H(a,v_{q'})\,]\,,\\
f_{qq'} &= -[\,F(a,v_q) - F(a,v_{q'})\,]\,.
\end{aligned} \tag{28}$$

The qq' contribution to the fractional polarization is then

$$\begin{aligned}
I_{qq'} &= \cos\alpha_{q-q'}\,\big[\,\big(\,h_{qq'}\,\cos\alpha_{q-q'} - f_{qq'}\,\sin\alpha_{q-q'}\,\big)\\
&\quad + i\,\big(\,h_{qq'}\,\sin\alpha_{q-q'} + f_{qq'}\,\cos\alpha_{q-q'}\,\big)\,\big]\,.
\end{aligned} \tag{29}$$

When the field strength is increased from zero ($\alpha_{q-q'} = 0$), the imaginary term increases from zero, while the real term decreases from a maximum value of $H(a,v)$. The real term is responsible for depolarization, the imaginary term for rotation. The wavelength dependence of these effects is contained in the $h_{qq'}$ and $f_{qq'}$ functions. The unpolarized case with $q,\,q' = 0$ is represented by $I_{00} = H(a,v)$ (since $\alpha_0 = 0$ and $f_{00} = 0$).

3. Transition of the Hanle effect from core to wings

Note that the above expressions are valid for any frequency and field strength. They are not limited to weak fields or to core or wing frequencies. No approximations are involved. We can use them to explore the transition of the Hanle effect from core to wings across the intermediate frequencies, as well as the transition from the Hanle to the ordinary Zeeman effect across the range of intermediate field strengths. All the intermediate regimes can be treated without approximations.

It has long been known from qualitative arguments that the Hanle effect is only effective in the Doppler core and disappears in the wings (cf. Stenflo 1994, p. 83), but only recently expressions have been found that describe the transition from core to wings. Due to partial redistribution the Hanle efficiency is a function of both the incident and scattered frequencies ν' and ν. Bommier (1997) has made 2-D diagrams that show this dependence in $\nu' - \nu$ space. As such complex diagrams are hard to read, we will here bring out in a more transparent fashion the essential property of this core-wing transition in a 1-D diagram as a function of a single frequency (for frequency-coherent scattering).

In the past, when deriving the weak-field Hanle phase matrix, one has factorized out the frequency dependent part (the complex Voigt functions) and in Eq. (26) made the approximation $\frac{1}{2}(\mathcal{H}_q + \mathcal{H}^*_{q'}) = H(a,v)$ when $\nu_L \ll \Delta\nu_D$. As the intensity contribution $I_{qq'}$ when $q,\,q' = 0$ is $I_{00} = H(a,v)$, the fractional polarization $I_{qq'}/I_{00}$ has then become $\cos\alpha_{q-q'}\,e^{i\alpha_{q-q'}}$, which is independent of frequency. The frequency dependence of the Hanle effect has thus been "thrown out", since the Hanle effect is not only contained in the Hanle angles $\alpha_{q-q'}$, but also in $\frac{1}{2}(\mathcal{H}_q + \mathcal{H}^*_{q'})$.

It is true that for small values of the Zeeman splitting the real part of $\frac{1}{2}(\mathcal{H}_q + \mathcal{H}^*_{q'})$ can be well approximated by $H(a,v)$, which does not contain any Hanle effect. It is however the imaginary part, in the form of $F_{q'} - F_q$, that carries the Hanle information and cannot be neglected.

In the past the function $f_{qq'}$ in Eq. (29) has thus been ignored, and $h_{qq'}$ has been approximated by $H(a,v)$, which implies removal of all the frequency variation of the Hanle effect. Let us now bring out this frequency variation explicitly and select the weak-field case for analytical simplicity. For intermediate or strong fields one would need to evaluate $I_{qq'}$ directly from Eq. (29).

For weak fields we can make the Taylor expansion

$$F(a,v_q) \approx F(a,v) - v_H\,\frac{\partial F(a,v)}{\partial v}\,, \tag{30}$$

and correspondingly for $H(a,v_q)$. To lowest order in v_H we only need to keep the first non-vanishing terms:

$$\begin{aligned}
h_{qq'} &\approx H(a,v)\,,\\
f_{qq'} &\approx (q-q')\,\frac{\partial F(a,v)}{\partial v}\,g_b\,\omega_L/\Delta\omega_D
\end{aligned} \tag{31}$$

(cf. Eq. (17)). As

$$\tan\alpha_{q-q'} = \frac{(q-q')\,g_b\,\omega_L/\Delta\omega_D}{2a}\,, \tag{32}$$

the term $(f_{qq'}/h_{qq'})\,\tan\alpha_{q-q'}$, which arises from the first bracket in Eq. (29), vanishes to first order in v_H or ω_L, while in the second bracket

$$\frac{f_{qq'}}{h_{qq'}}\,\cot\alpha_{q-q'} \approx 2a\,\frac{\partial F(a,v)}{\partial v}\,\Big/\,H(a,v)\,. \tag{33}$$

Then, to first order in v_H,

$$\begin{aligned}
\frac{I_{qq'}}{I_{00}} &= \cos^2\alpha_{q-q'}\\
&\quad + \,0.5\,i\sin 2\alpha_{q-q'}\,\Big[1 + 2a\,\frac{\partial F(a,v)}{\partial v}\,\Big/\,H(a,v)\,\Big]\,.
\end{aligned} \tag{34}$$

The relative wavelength variation of the Hanle rotation efficiency is contained in the function in the square bracket. This function is plotted in Fig. 1 for various values of the damping parameter a. For small values of a the Hanle efficiency extends

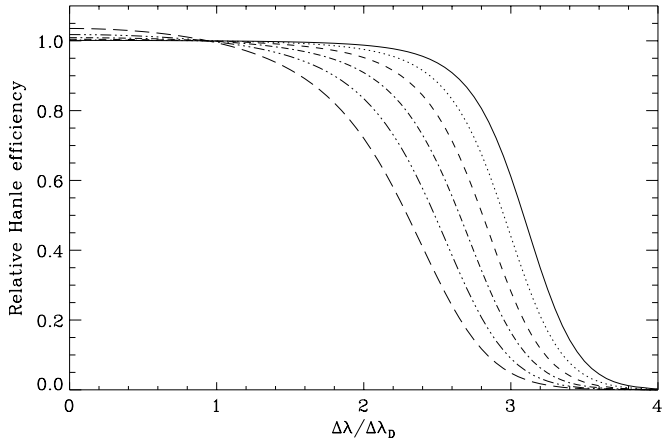

Fig. 1. Relative Hanle efficiency, represented by the function in the square bracket of Eq. (34), as a function of distance $v = \Delta\lambda/\Delta\lambda_D$ from line center. The various curves represent different values of the damping parameter a in a progression from right to left. The rightmost (solid) curve corresponds to $a = 0.001$, then follow the curves for $a = 0.002$, 0.004, 0.008, 0.016, and 0.032.

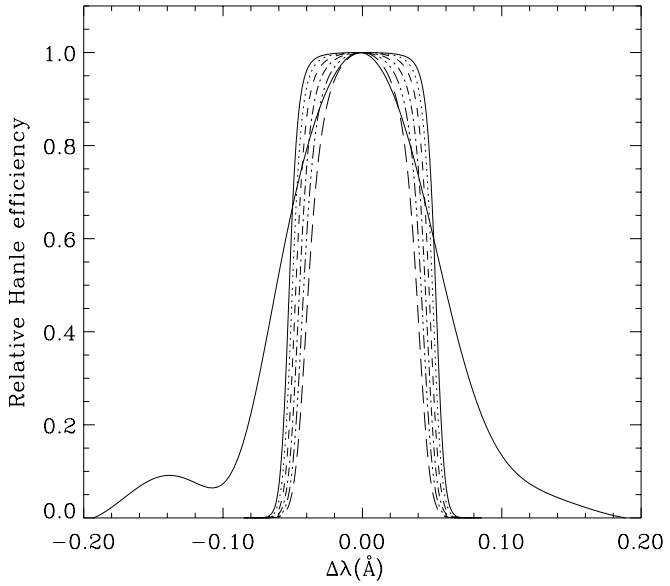

Fig. 2. Comparison between theory and observations for the relative Hanle efficiency. The six theoretical curves are the same as in Fig. 1, but the wavelength scale has been converted to Å assuming a Doppler width of 1.25 km s^{-1} in velocity units. The observational curve (solid line) is based on observations of the Stokes U/Q ratio in the Sr II 4078 Å line (Bianda et al. 1998). All curves have been normalized to a maximum value of unity. No attempt has been made to apply instrumental broadening to the theoretical curves.

with full amplitude to a distance of about three Doppler widths from the line center, but this range decreases with increasing a.

Although the Hanle depolarization only enters at second order or higher in v_H, its relative variation with frequency is governed by the same profile function, $f_{qq'}/h_{qq'}$, as the Hanle rotation, as seen by Eq. (29).

Recently Bianda et al. (1998) have determined empirical Hanle efficiency profiles through Stokes Q and U observations in the Sr II 4078 Å line. In Fig. 2 we compare the empirical efficiency profile (solid curve), taken from Fig. 13a in Bianda et al. (1998), with the same set of theoretical profiles that were displayed in Fig. 1, assuming a Doppler width of 1.25 km s^{-1} in velocity units. Part of the difference in shape between the empirical and theoretical curves may be understood in terms of instrumental broadening, which affects the observations but has not been applied to smear the theoretical curves. With reasonable values for the instrumental broadening a much closer fit between theory and observations could be obtained, but such detailed modelling is not needed at this stage.

Let us for clarity here comment on the conceptual connection between the empirical and theoretical curves. Much of this will become clearer in the following sections, but we summarize the arguments here. The empirical curve represents the ratio between the mean observed Stokes U and Q line profiles. This can be simulated by forming the ratio between the solid (weak-field) theoretical curves in the lower and upper right panels of Fig. 4 below. Since the line contribution to Q is spectrally flat in the limit of weak fields (cf. the solid curve in the upper right panel of Fig. 3 below), the ratio between the U and Q curves with background continuum included is proportional to the line contribution to U, which is represented by the profiles of Fig. 1 in the weak-field limit.

4. Analytical form of the Hanle-Zeeman scattering matrix

I have developed a computer program that allows the Hanle-Zeeman scattering matrix $\boldsymbol{M}$ to be computed from the equations of Sect. 2 for the general case of arbitrary atomic multiplets, with or without hyperfine structure splitting, allowing for the initial and final states to be different (Raman scattering), for arbitrary magnetic fields, frequencies, and scattering geometries (the field does not have to be along the polar axis).

Although thus any scattering problem can be treated by numerical computation (assuming that the initial-state atomic polarization is either zero or given by the solution of the statistical equilibrium problem), the computer program is like a "black box" inside which the physics is hidden. To make the physics more visible it is very useful to have a compact, analytical representation of the scattering matrix. Such a representation can also directly show how the various special, limiting cases follow from the general formulation, and it allows us to see what happens in the intermediate regime that represents the transition between these limiting cases.

For clarity and compactness we have derived this analytical representation of the Hanle-Zeeman scattering matrix for the special case of a normal Zeeman triplet only (a $J = 0 \rightarrow 1 \rightarrow 0$ scattering transition), but it is valid for arbitrary magnetic field strengths and directions (for a coordinate system in which the polar axis is along the magnetic field). To simplify the expressions let us introduce the quantities $c_{qq'}$ and $s_{qq'}$:

$$c_{qq'} \;=\; \cos\alpha_{q-q'}\,\big\{\,\cos\left[(q-q')(\phi-\phi')\right]$$

$$
\begin{aligned}
&(h_{qq'} \cos\alpha_{q-q'} - f_{qq'} \sin\alpha_{q-q'}) + \sin[(q-q')(\phi-\phi')] \\
&(h_{qq'} \sin\alpha_{q-q'} + f_{qq'} \cos\alpha_{q-q'}) \big\} , \\
s_{qq'} \;=\; &\cos\alpha_{q-q'} \big\{ \sin[(q-q')(\phi-\phi')] \\
&(h_{qq'} \cos\alpha_{q-q'} - f_{qq'} \sin\alpha_{q-q'}) - \cos[(q-q')(\phi-\phi')] \\
&(h_{qq'} \sin\alpha_{q-q'} + f_{qq'} \cos\alpha_{q-q'}) \big\} . \qquad (35)
\end{aligned}
$$

Note that $c_{qq'}$ and $s_{qq'}$ obey the symmetries

$$
\begin{aligned}
c_{qq'} \;&=\; c_{q'q} \,, \\
s_{qq'} \;&=\; -s_{q'q} \,. \qquad (36)
\end{aligned}
$$

Let us for convenience introduce the notations

$$
\begin{aligned}
c_0^0 \;&=\; c_{00} \,, \\
c_\pm^0 \;&=\; \tfrac{1}{2}(c_{11} \pm c_{-1,-1}) \,, \\
c_\pm^1 \;&=\; \tfrac{1}{2}(c_{10} \pm c_{0,-1}) \,, \qquad (37) \\
c_+^2 \;&=\; c_{1,-1}
\end{aligned}
$$

and correspondingly for s_r^K ($r = 0, \pm$, $K = 0, 1, 2$). The expressions for c_r^0 are particularly simple:

$$
\begin{aligned}
c_0^0 \;&=\; H_0 \,, \\
c_\pm^0 \;&=\; \tfrac{1}{2}(H_+ \pm H_-) \,, \qquad (38)
\end{aligned}
$$

where

$$
H_q = H(a, v_q) \,. \qquad (39)
$$

Let us further introduce the matrices

$$
\boldsymbol{C}_0^0 = (1-\mu^2)(1-\mu'^2) \begin{pmatrix} 1 & 1 & 0 & 0 \\ 1 & 1 & 0 & 0 \\ 0 & 0 & 0 & 0 \\ 0 & 0 & 0 & 0 \end{pmatrix} , \qquad (40)
$$

$$
\boldsymbol{C}_+^0 = \frac{1}{2} \qquad (41)
$$

$$
\begin{pmatrix} (1+\mu^2)(1+\mu'^2) & -(1+\mu^2)(1-\mu'^2) & 0 & 0 \\ -(1-\mu^2)(1+\mu'^2) & (1-\mu^2)(1-\mu'^2) & 0 & 0 \\ 0 & 0 & 0 & 0 \\ 0 & 0 & 0 & 4\mu\mu' \end{pmatrix} ,
$$

$$
\boldsymbol{C}_-^0 = \begin{pmatrix} 0 & 0 & 0 & (1+\mu^2)\mu' \\ 0 & 0 & 0 & -(1-\mu^2)\mu' \\ 0 & 0 & 0 & 0 \\ \mu(1+\mu'^2) & -\mu(1-\mu'^2) & 0 & 0 \end{pmatrix} , \qquad (42)
$$

$$
\boldsymbol{C}_+^2 = \frac{1}{2} \qquad (43)
$$

$$
\begin{pmatrix} (1-\mu^2)(1-\mu'^2) & -(1-\mu^2)(1+\mu'^2) & 0 & 0 \\ -(1+\mu^2)(1-\mu'^2) & (1+\mu^2)(1+\mu'^2) & 0 & 0 \\ 0 & 0 & 4\mu\mu' & 0 \\ 0 & 0 & 0 & 0 \end{pmatrix} ,
$$

$$
\boldsymbol{S}_+^2 = \begin{pmatrix} 0 & 0 & -(1-\mu^2)\mu' & 0 \\ 0 & 0 & (1+\mu^2)\mu' & 0 \\ \mu(1-\mu'^2) & -\mu(1+\mu'^2) & 0 & 0 \\ 0 & 0 & 0 & 0 \end{pmatrix} , \qquad (44)
$$

$$
\boldsymbol{C}_+^1 = \mu\mu' \begin{pmatrix} 1 & 1 & 0 & 0 \\ 1 & 1 & 0 & 0 \\ 0 & 0 & 0 & 0 \\ 0 & 0 & 0 & 0 \end{pmatrix} + \boldsymbol{E}_{33} + \boldsymbol{E}_{44} \,, \qquad (45)
$$

$$
\boldsymbol{C}_-^1 = \begin{pmatrix} 0 & 0 & 0 & \mu \\ 0 & 0 & 0 & \mu \\ 0 & 0 & 0 & 0 \\ \mu' & \mu' & 0 & 0 \end{pmatrix} , \qquad (46)
$$

$$
\boldsymbol{S}_+^1 = \begin{pmatrix} 0 & 0 & \mu & 0 \\ 0 & 0 & \mu & 0 \\ -\mu' & -\mu' & 0 & 0 \\ 0 & 0 & 0 & 0 \end{pmatrix} , \qquad (47)
$$

$$
\boldsymbol{S}_-^1 = \boldsymbol{E}_{43} - \boldsymbol{E}_{34} \,. \qquad (48)
$$

Here $\boldsymbol{E}_{ij}$ denotes a matrix that has the single element $E_{ij} = 1$, while all the remaining elements are zero.

With these various notations we can now write the general Hanle-Zeeman scattering matrix $\boldsymbol{M}$ in the compact form

$$
\begin{aligned}
\boldsymbol{M} \;=\; &\tfrac{3}{4}(c_0^0 \boldsymbol{C}_0^0 + c_+^0 \boldsymbol{C}_+^0 + c_-^0 \boldsymbol{C}_-^0 + c_+^2 \boldsymbol{C}_+^2 + s_+^2 \boldsymbol{S}_+^2) \\
&+ \tfrac{3}{2} \sin\theta \sin\theta' \, (c_+^1 \boldsymbol{C}_+^1 + c_-^1 \boldsymbol{C}_-^1 + s_+^1 \boldsymbol{S}_+^1 + s_-^1 \boldsymbol{S}_-^1) \,. \qquad (49)
\end{aligned}
$$

5. Special cases

5.1. Weak-field Hanle phase matrix

The well-known weak-field Hanle phase matrix is retrieved from Eqs. (13) or (49) if we in addition to going to the limit of weak fields set $f_{qq'} = 0$ (i.e., ignore anomalous dispersion). Then the frequency dependence of all the matrix elements in $\boldsymbol{M}$ become identical and equal to $h_{qq'} = H(a, v)$, so that $\boldsymbol{M}$ can be written as $H(a, v)\boldsymbol{P}$, where $\boldsymbol{P}$ is a frequency-independent phase matrix. As pointed out in Sect. 3, it is the (incorrect) omission of $f_{qq'}$ when deriving the weak-field limit that makes the phase matrix frequency independent. It is $f_{qq'}$ that contains the property that the Hanle effect is present in the line core but absent in the line wings.

As readily seen from Eqs. (35)–(38) and (49) we obtain for a $J = 0 \to 1 \to 0$ scattering transition in the weak-field limit when omitting $f_{qq'}$

$$
\begin{aligned}
\boldsymbol{M}/H_0 \;&=\; \tfrac{3}{4}(\boldsymbol{C}_0^0 + \boldsymbol{C}_+^0 + c_\alpha^2 \boldsymbol{C}_+^2 + s_\alpha^2 \boldsymbol{S}_+^2) \\
&+\; \tfrac{3}{2} \sin\theta \sin\theta' \, (c_\alpha^1 \boldsymbol{C}_+^1 + s_\alpha^1 \boldsymbol{S}_+^1) \,, \qquad (50)
\end{aligned}
$$

where

$$
\begin{aligned}
c_\alpha^K \;&=\; \cos\alpha_K \cos[K(\phi-\phi') - \alpha_K] \,, \\
s_\alpha^K \;&=\; \cos\alpha_K \sin[K(\phi-\phi') - \alpha_K] \,. \qquad (51)
\end{aligned}
$$

It is easy to verify that the matrix represented by $\boldsymbol{M}/H_0$ in Eq. (50) is identical to the Hanle weak-field phase matrix given in Stenflo (1994, pp. 88–89), except for a small error in the previously published (Stenflo 1978, 1994) versions of this phase matrix: The coefficient for $\mu\mu'$ that appears in the matrix position P_{44} (in Eq. (5.58) in Stenflo 1994) is too small by a factor of two.

For a general Raman scattering transition in an arbitrary atomic multiplet we retrieve in the zero-field limit the theory that was developed in Stenflo (1997).

5.2. Coronal forbidden lines

Due to the extraordinarily long life times of the excited states of forbidden lines, the Zeeman splitting exceeds the natural line width already for microgauss fields. Since all coronal magnetic fields are much stronger than microgauss, we are always in the strong-field regime (with respect to the Hanle effect in forbidden lines) in the solar corona. There are no coherences or overlap between the Zeeman sublevels.

As follows from Eq. (21), this limiting case is obtained by letting the Hanle angles $\alpha_{q-q'} \rightarrow \pi/2$. Then both $c_{qq'}$ and $s_{qq'}$ in Eq. (35) vanish whenever $q \neq q'$, so that only c^0_r, $r = 0, \pm$, survive, while $c^{1,2}_r$ and all s^K_r do not. The remaining terms give in this strong-field limit

$$\boldsymbol{M}_{\rm strong} = \tfrac{3}{4}[\, H_0 \boldsymbol{C}^0_0 \;+\; \tfrac{1}{2}(H_+ + H_-)\boldsymbol{C}^0_+ + \;\tfrac{1}{2}(H_+ - H_-)\boldsymbol{C}^0_-\,]\,. \tag{52}$$

Since the Zeeman splitting is much smaller than the Doppler width for the coronal forbidden lines, we have $H_\pm \approx H_0$, so that

$$\boldsymbol{M}_{\rm corona}/H_0 = \tfrac{3}{4}(\boldsymbol{C}^0_0 + \boldsymbol{C}^0_+) = \boldsymbol{E}_{11} \;+\; \tfrac{3}{8} \;\times \tag{53}$$
$$\begin{pmatrix} \frac{1}{3}(1-3\mu^2)(1-3\mu'^2) & (1-3\mu^2)(1-\mu'^2) & 0 & 0 \\ (1-\mu^2)(1-3\mu'^2) & 3(1-\mu^2)(1-\mu'^2) & 0 & 0 \\ 0 & 0 & 0 & 0 \\ 0 & 0 & 0 & 4\mu\mu' \end{pmatrix}.$$

We see from the structure of this matrix that incident unpolarized radiation acquires, through the scattering process, a Stokes Q linear polarization that is proportional to $1 - 3\cos^2\theta'$, where θ' is the angle between the incident radiation and the magnetic-field vector. When

$$\cos^2\theta' = 1/3\,, \tag{54}$$

i.e., when $\theta' = 54\overset{\circ}{.}7$, which is the so-called Van Vleck angle (Van Vleck 1925; House 1974), the polarization undergoes a sign change. When θ' is smaller than the Van Vleck angle, the linear polarization is perpendicular to the direction of the magnetic field (projected on the plane of the sky), when the angle is larger, the polarization of the scattered radiation is parallel to the projected field direction.

5.3. Thermal radiation limit

The term "thermal radiation limit" here refers to the case when, at the time of the emission process, the radiating atom has lost all its memory about how it was excited. Such a memory loss can have different causes. The atom may for instance during the scattering process have had a collision that destroyed the polarization of the excited state. We then get *incoherent* scattering. Alternatively, the upper state may have been populated by processes other than radiative excitation, e.g. non-directional collisional excitation or recombination. All such processes that carry no directional information should all lead to the same polarization form for the Stokes emission vector.

As there is no "memory" about the excitation process, the "thermal" emission vector $\boldsymbol{j}_{\rm th}$ is obtained from Eq. (13) for the general Hanle-Zeeman scattering matrix $\boldsymbol{M}$ for arbitrary magnetic fields, geometries, and atomic multiplets by calculating the scattered Stokes vector for the case when the incident radiation is unpolarized and isotropic. Thus

$$\boldsymbol{j}_{\rm th} \sim \langle \boldsymbol{M} \rangle' \begin{pmatrix} 1 \\ 0 \\ 0 \\ 0 \end{pmatrix}\,, \tag{55}$$

where $\langle\;\rangle'$ symbolizes averaging over all angles of incidence (while keeping the directions of the magnetic field and the scattered radiation fixed).

For the special case of a normal Zeeman triplet we see from Eq. (35) that $c_{qq'}$ and $s_{qq'}$ vanish for $q \neq q'$ when averaging over all azimuth angles. Like for the strong-field case of Sect. 5.2 only the coefficients c^0_r, $r = 0, \pm$, survive. After azimuth averaging the resulting matrix thus has the same form as $\boldsymbol{M}_{\rm strong}$. As the average of μ'^2 is $\frac{1}{3}$, the subsequent averaging over all colatitudes θ' gives (only the first column of $\boldsymbol{M}$ matters for the "thermal limit")

$$\boldsymbol{j}_{\rm th} \sim \begin{pmatrix} H_I \\ H_Q \\ H_U \\ H_V \end{pmatrix}\,, \tag{56}$$

where

$$\begin{aligned} H_I &= H_\Delta(1-\mu^2) + \tfrac{1}{2}(H_+ + H_-)\,, \\ H_Q &= H_\Delta(1-\mu^2)\cos 2\chi\,, \\ H_U &= H_\Delta(1-\mu^2)\sin 2\chi\,, \\ H_V &= \tfrac{1}{2}(H_+ - H_-)\,\mu\,, \\ H_\Delta &= \tfrac{1}{2}[\,H_0 - \tfrac{1}{2}(H_+ + H_-)\,] \end{aligned} \tag{57}$$

as in Stenflo (1994, Eqs. (4.36), (4.48), and (4.49)). However, with the definition of the Stokes vector coordinate system used here, $\chi = 0$, so that $H_U = 0$.

For the general case, Eq. (13), for arbitrary atomic multiplets, the same procedure of averaging $\boldsymbol{M}$ leads to a $\boldsymbol{j}_{\rm th}$, where $H_{I,Q,U,V}$ are replaced by the sum over the contributions to the corresponding quantities from the various π and σ components within the anomalous Zeeman splitting pattern, weighted by the relative transition strengths of the Zeeman components (cf. Stenflo 1994, pp. 107–115).

6. Transition between the Hanle and Zeeman effects

The relative importance of the Hanle and Zeeman effects depends on the field strength, inclination, scattering geometry, and collision rate. The theory that we have presented accounts for all these dependencies. To convey a feeling for the general behavior of the Mueller scattering matrix we will illustrate the Stokes profiles for a sequence of field strengths for an atomic transition of the $J = 0 \rightarrow 1 \rightarrow 0$ type (corresponding to classical dipole scattering) and a scattering angle of 90°. We assume that the magnetic field is canopy-like and lies in the horizontal

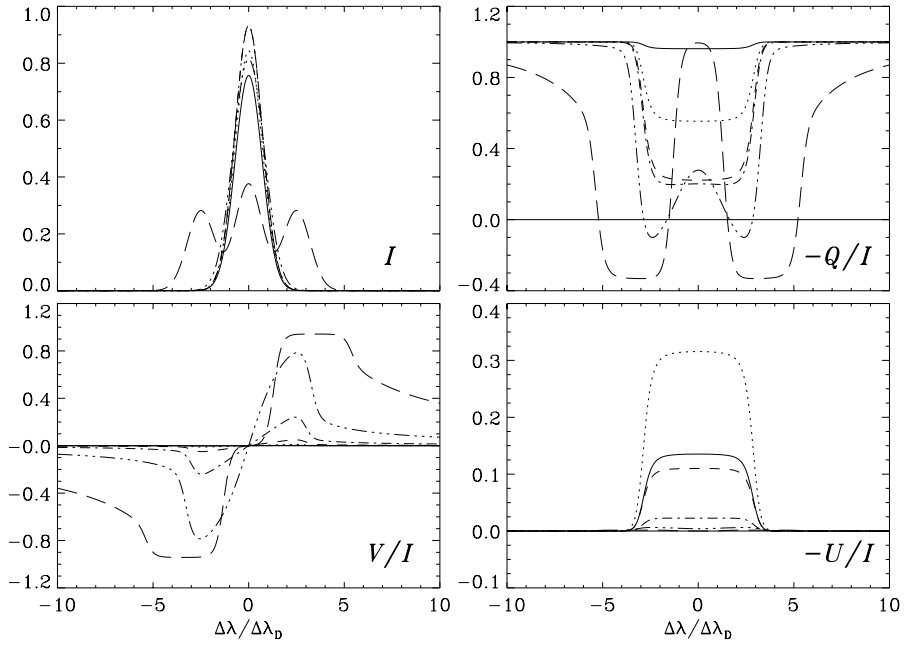

Fig. 3. Illustration of the transition from the Hanle to the Zeeman effect when the magnetic field is in the horizontal plane and at 45° to the observer, and the field strength parameter v_H increases from 0.0008 (solid curves) in steps of a factor of 5 to reach 2.5 for the long-dash curves. Single 90° scattering of unpolarized radiation at the extreme limb is assumed. The profiles of the intensity or scattering probability I and the fractional polarizations Q/I, U/I, and V/I are plotted. Note, however, that these profiles characterize scattering in an isolated spectral line without any continuum radiation.

plane. The line of sight is also assumed to lie in the horizontal plane (which is the case when the observations refer to the extreme limb of the Sun) at an angle of 45° to the field direction. The incident radiation is assumed to be unpolarized and in the vertical direction (which represents the idealized case of extreme limb darkening).

By choosing the magnetic field to be in the horizontal plane we optimize the conditions for the Hanle effect to manifest itself (since the Hanle effect vanishes for a vertical magnetic field). By choosing a 45° direction with respect to the line of sight we allow both the longitudinal and transverse Zeeman effects to make themselves seen.

In Fig. 3 we plot the results for the Mueller scattering matrix $\boldsymbol{M}$ in Eq. (49). The matrix has been normalized such that the isotropic part of M_{11} equals unity. I, Q, U, V in the figure are represented by M_{11}, M_{21}, M_{31}, and M_{41}, respectively. The fractional polarization U/I is for instance given by M_{31}/M_{11}. These are the fractional polarizations that result from a single scattering process in the line when the incident radiation is unpolarized. The Stokes I (i.e., M_{11}) profiles describe the wavelength variation of the scattering probability.

The various curves represent a sequence of increasing magnetic field strength, defined by the splitting parameter v_H of Eq. (17). The field strength increases by a *factor* of 5 between each curve. Thus the solid curve has $v_H = 0.0008$, the dotted curve has 0.004, the dashed curve 0.02, the dash-dot curve 0.1, the dash-dot-dot-dot curve 0.5, and the long-dash curve $v_H = 2.5$. We thus span a dynamic range with a ratio of 3125 between the highest and lowest field strengths. The damping constant a is assumed to be 0.004, the wavelength 5000 Å, and the Doppler width 30 mÅ.

Fig. 3 shows that the scattering probability function (I) does not alter its shape much until the Zeeman splitting gets quite large ($v_H \gtrsim 1$). The non-magnetic scattering polarization appears exclusively in Stokes Q, with $-Q/I = 1$ independent of frequency. Note, however, that although the non-magnetic polarization remains 100 % in the far wings, we run out of photons when the scattering probability approaches zero, as it does when we move away from the line center.

$-U/I$ has no contribution from the transverse Zeeman effect and is produced exclusively by Hanle rotation of the plane of linear polarization. The U/I profile shape illustrates nicely how the Hanle effect vanishes in the line wings at $v \approx 3$, as shown in more detail in Fig. 1. For weak fields the U/I polarization first increases (the dotted curve has a much larger amplitude than the solid one) and then decreases towards zero. U/I is thus large only within a rather well-defined range of weak fields.

As the field strength increases, the Q/I scattering polarization is first depolarized with a frequency profile for the depolarization effect that has the same shape as the U/I profile, again illustrating how the Hanle effect disappears in the line wings. For strong fields the signature of the transverse Zeeman effect emerges.

V/I is zero in the absence of magnetic fields but develops an anti-symmetric profile of increasing amplitude as the field strength increases, as expected. For strong fields the profile saturates at $V/I = 100$ % , but the deformed and extended profile shape is a property of the fractional polarization V/I, not of Stokes V alone.

In a real solar spectrum the line emission is superposed on a background of continuous emission that is weakly polarized by non-magnetic Rayleigh scattering (at neutral hydrogen and at free electrons). The relative importance of the line emission scales with $I/(I+a)$, where I represents the scattering probability as before, and a is a constant that represents the background continuum. This weighting function approaches zero in the line wings, since the scattering probability approaches zero while the continuum level remains constant.

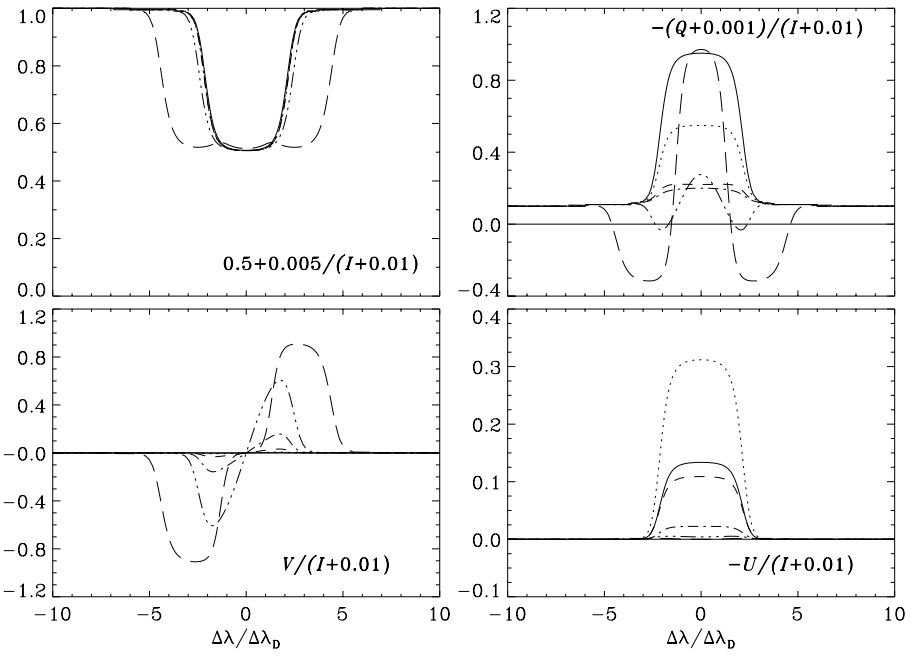

Fig. 4. Illustration of the transition from the Hanle to the Zeeman effect in a spectral line, in the presence of continuum radiation. The polarized profiles have been obtained from the Q, U, and V data in Fig. 3 using Eq. (58), with $a = 0.01$, and $b = 0.1$ (for Stokes Q) or 0 (for Stokes U and V). The intensity profiles in the upper left panel have been obtained from a simple Milne-Eddington model and Eq. (61) with $a = 0.01$ and $\beta = 0.5$. The magnetic-field parameters and the scattering geometry are the same as in Fig. 3.

Let p represent the fractional polarization in the form of $-Q/I$, $-U/I$, or V/I. Then the "observed" polarization p' in the presence of a continuum background can be written

$$p' = \frac{I}{I+a}\, p + \frac{a}{I+a}\, b\,, \tag{58}$$

where b represents the non-magnetic polarization of the background continuum. For symmetry reasons b is only non-zero for Q/I.

To model the emergent Stokes I in the presence of a continuous spectrum in a plausible way without entering into radiative-transfer calculations, we assume LTE (thermal radiation) and make use of the Milne-Eddington model, according to which (Stenflo 1994, pp. 249-250)

$$I'/I'_c = 1 - \beta + \frac{\beta}{\eta_0 H_I + 1} \tag{59}$$

(note that Eq. (11.59) in Stenflo (1994) contains a sign error for β), where H_I is given by Eq. (57), η_0 is the ratio between the absorption coefficients at line center and in the continuum, and β is a limb-darkening parameter (with a value between 0 and 1) determined by the temperature gradient in the line-forming layers.

The justification for using a Milne-Eddington model for Stokes I although such a model has nothing to do with scattering is that much of the intensity spectrum is formed by processes other than coherent scattering, in contrast to the fractional polarization for weak magnetic fields. It is the fractional polarization that we are interested in here. It is treated in the last scattering approximation, as a single scattering event superposed on a continuous background. The intensity spectrum on the other hand is dominated by optical depth effects, so that the use of some radiative transfer solution becomes unavoidable. For stronger fields, when the Zeeman effect comes into play, optical-depth effects (via the Mueller absorption matrix) will become important also for the polarized profiles and should be accounted for in a more complete treatment. This is however outside the scope of the present paper, in which we focus the attention exclusively on the Mueller *scattering* matrix.

In the LTE or "thermal radiation" limit our I is $\sim H_I$ as shown by Eq. (56). With a suitable choice of η_0 we can always achieve that

$$I = a\eta_0 H_I\,. \tag{60}$$

In this case

$$I'/I'_c = 1 - \beta + \frac{a}{I+a}\,\beta\,. \tag{61}$$

For illustrative purposes we will use this expression also when I refers to the general non-LTE case with coherent scattering.

In Fig. 4 we give I'/I'_c and p' ($= -Q'/I', -U'/I', V'/I'$) based on the I, Q, U, and V in Fig. 3, for the parameter choice $a = 0.01$, $b = 0.1$, and $\beta = 0.5$. The profile shapes in Fig. 4 are more realistic than in Fig. 3, with the far line wings of the p' diagrams being suppressed by the continuum radiation. The non-magnetic $-Q'/I'$ polarization is now elevated only in the line core and approaches the continuum polarization value b in the far wings. The line polarization is depolarized by the Hanle effect as the field strength increases, until the transverse Zeeman effect starts to become significant and subsequently dominates the profile shape. The behavior of U'/I' and V'/I' is similar to that of U/I and V/I in Fig. 3, except for the suppression and rounding-off of the far-wing polarization. The I'/I'_c profile is considerably broader than the I profile, and only for strong fields ($v_H \gtrsim 1$) the Zeeman splitting begins to affect the line shape.

7. Conclusions

Magnetic fields affect the polarization that is produced by coherent scattering in different ways. In the regime of weak fields the Hanle effect dominates, while for strong fields the usual Zeeman effect determines the polarization. In the general case there are mixed contributions from both effects. These contributions also vary in different ways with frequency from line core to wings, and they depend on the quantum numbers of the atomic transitions involved and on the type of scattering transition (Rayleigh scattering, when the initial and final states are the same, and Raman scattering, when they are different). All these various parameter combinations provide us with rich diagnostic opportunities, and highly sensitive imaging vector polarimeters are being developed that may allow the new diagnostic possibilities to be exploited. We therefore now need adequate theoretical tools to be able to interpret the wealth of new data that will be forthcoming.

In the present paper we have developed a theoretical framework for the convenient calculation of the Mueller scattering matrix for arbitrary magnetic fields, atomic multiplets, and scattering processes. For the special case of a normal Zeeman triplet (a $J = 0 \rightarrow 1 \rightarrow 0$ scattering transition) we have expressed this scattering matrix in a compact analytical form, which aids the physical understanding and allows us to better see how the various special regimes follow from the general matrix.

We have demonstrated how common limiting cases may be retrieved from the general theory, like the weak-field Hanle phase matrix, including the functional form of the variation of the Hanle efficiency from core to wings, the polarization of coronal forbidden lines, thermal radiation (the emission vector in the Unno 1956 theory), and incoherent scattering. We have also illustrated how the Stokes profiles change when we make the transition from the weak-field Hanle effect to the Zeeman effect by gradually increasing the magnetic field strength. Effects of partial frequency redistribution (PRD) are however left out in the present treatment (in contrast to the recent work by Bommier (1997), who has developed the general theoretical framework for dealing with PRD in the presence of arbitrary magnetic fields).

For the interpretation of real observations our general Mueller scattering matrix needs to be used in a radiative transfer equation, the solution of which is a major numerical problem. Recently advanced numerical techniques with accelerated lambda iteration have been developed to solve the vector radiative transfer equation when the weak-field Hanle phase matrix is included (Nagendra et al. 1998).

References

Bianda, M., Stenflo, J.O., Solanki, S.K. 1998, A&A 337, in press
Bommier, V., 1997, A&A 328, 726
House, L.L., 1974, PASP 86, 490
Landi Degl'Innocenti, E., 1998, Nature 392, 256
Nagendra, K.N., Frisch, H., Faurobert-Scholl, M., 1998, A&A 332, 610
Stenflo, J.O., 1978, A&A 66, 241
Stenflo, J.O., 1994, Solar Magnetic Fields – Polarized Radiation Diagnostics. Kluwer, Dordrecht
Stenflo, J.O., 1997, A&A 324, 344
Stenflo, J.O., Keller, C.U., 1996, Nature 382, 588
Stenflo, J.O, Keller, C.U., 1997, A&A, 321, 927
Stenflo, J.O, Keller, C.U., Gandorfer, A., 1998, A&A, 329, 319
Trujillo Bueno, J., Landi Degl'Innocenti, E., 1997, ApJ 482, L183
Unno, W., 1956, PASJ 8, 108
Van Vleck, J.H., 1925, Proc. Nat. Acad. Sci. 11, 612